eLIFE
elifesciences.org

Figures and figure supplements

Cross-synaptic synchrony and transmission of signal and noise across the mouse retina

William N Grimes, et al.

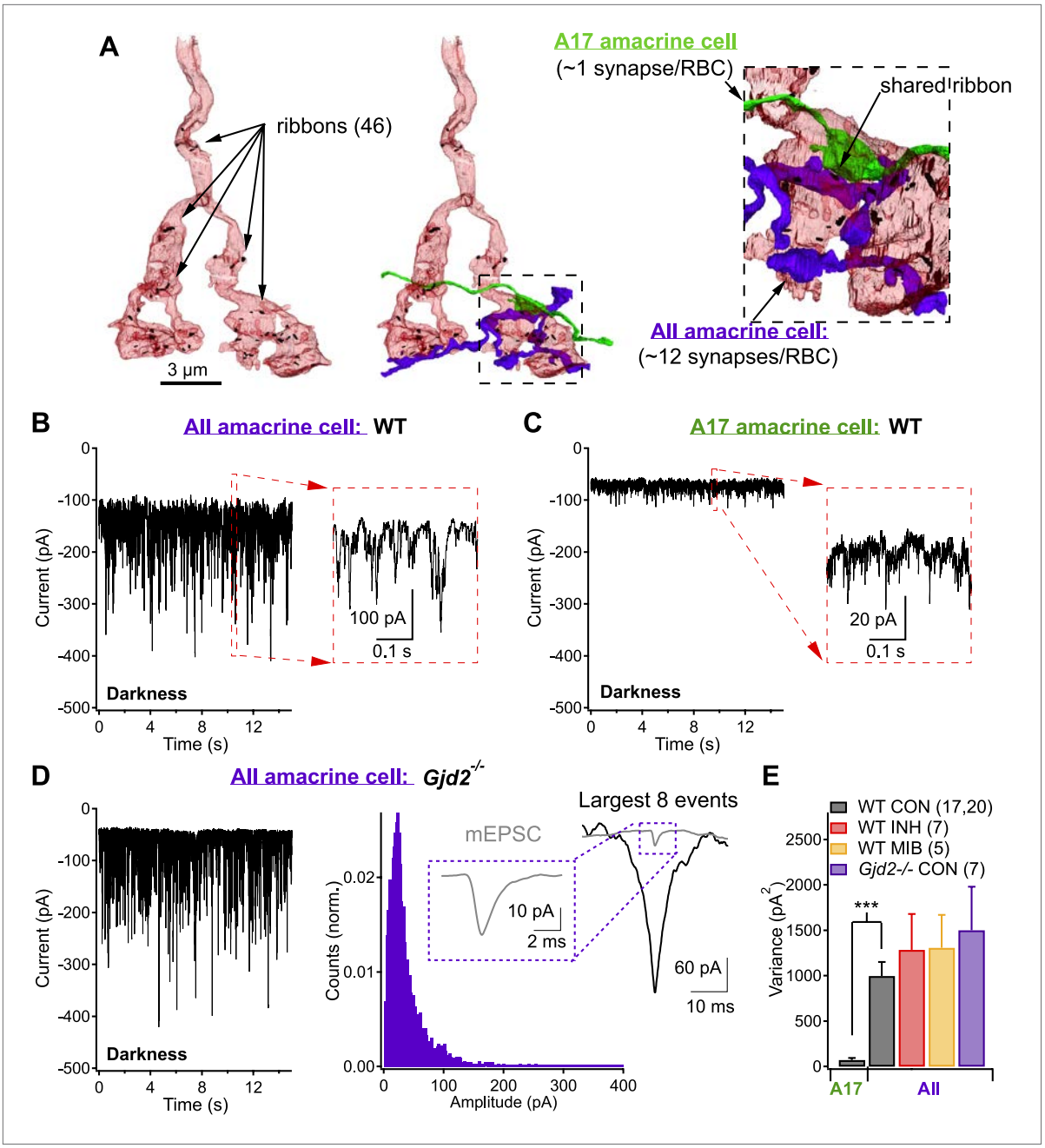

Figure 1. Same presynaptic neuron, very different postsynaptic noise properties. (**A**) Three-dimensional EM reconstruction of a rod bipolar cell axon terminal (pink), presynaptic ribbons are represented with black markers (46 in total). AII (purple) and A17 (green) amacrine cells are complimentary postsynaptic partners at individual RBC ribbon synapses, but unlike the A17, AIIs receive synaptic input from multiple presynaptic ribbons. (**B** and **C**) Voltage-clamp recordings from AII (**B**) and A17 (**C**) amacrine cells (V_{hold} ~−60 mV) in retinas from wild-type mice demonstrate that tonic excitatory synaptic input (from RBCs) to these two cell types can be very different under physiological recording conditions. Under dark-adapted conditions large noise events are observed at RBC→AII connections (**B**) but not at RBC→A17 connections (**C**). (**D**) AII recordings from retinal slices lacking Cx36-containing gap junctions (i.e., *Gjd2* knockout mouse, where electrical synapses between AII amacrine cell dendrites and On cone bipolar axon terminals have been eliminated) exhibited similar behavior to recordings from wild-type retina. Under these conditions synaptic events were analyzed. Inset: fast synaptic events (with 10–90% rise time ≤1 ms, i.e., miniature excitatory postsynaptic current or mEPSC) exhibited amplitudes that were less than a tenth of that of the largest events. (**E**) Population statistics for the synaptic noise recorded from AII and A17 amacrine cells in wild type and *Gjd2*$^{-/-}$ recordings under dark-adapted conditions (control or drugs). On average, noise recorded from AII amacrine cells (WT) was >10 times larger than noise recorded from A17 amacrine cells (unpaired *t* test $p = 3 \times 10^{-6}$). Neither an inhibitory cocktail (2 µM Strychnine, 20 µM SR95531 and 50 µM TPMPA) or mibefridil (10 µM, T-type Ca_v channel antagonist) caused a significant change in the noise recorded from AII amacrine cells in darkness.

DOI: 10.7554/eLife.03892.003

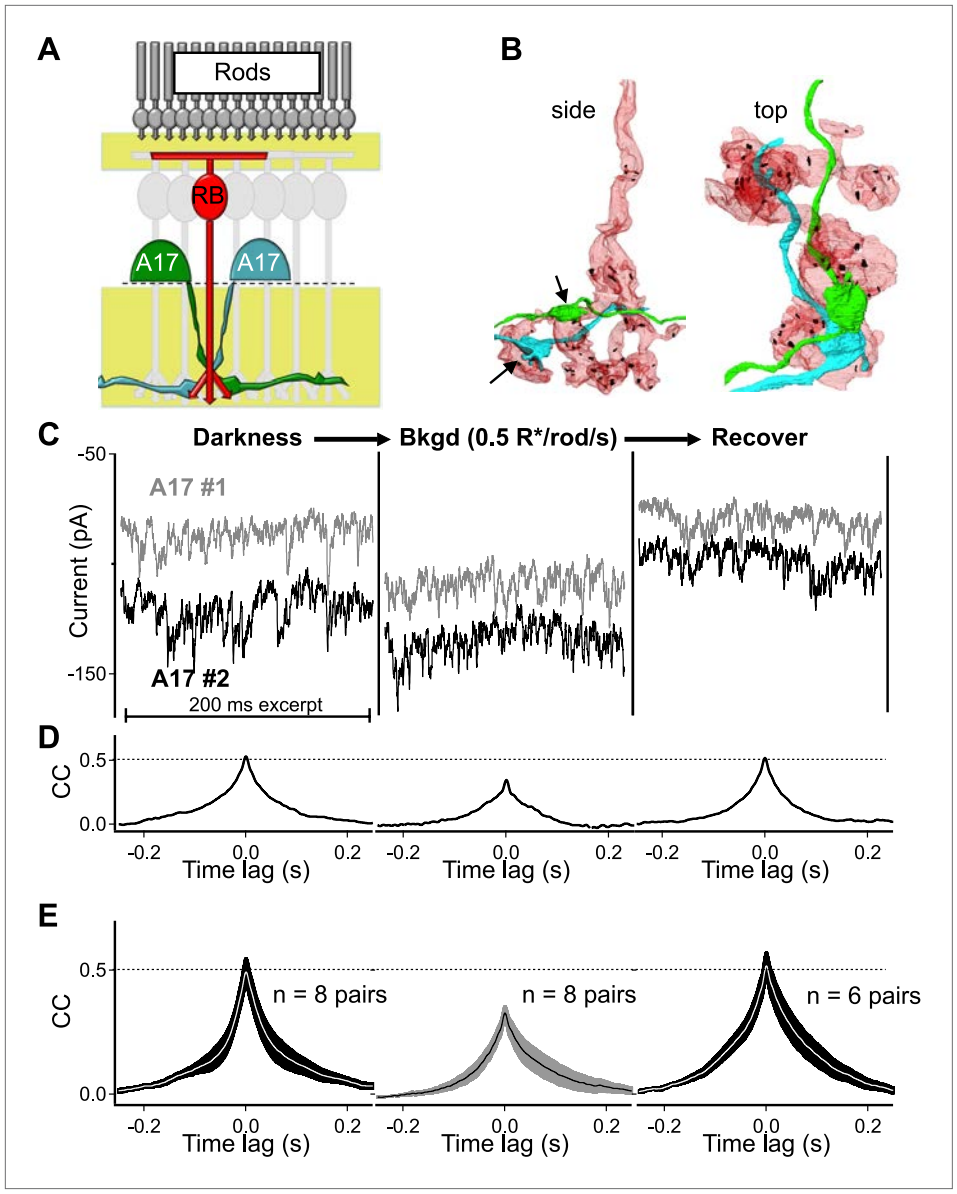

Figure 2. Strong covariation in overlapping A17 amacrine cells reflects highly synchronized cross-synaptic release from individual RBCs under dark-adapted conditions. (**A**) Paired recordings from neighboring A17 amacrine cells in the wild type retinal slice preparation were used to measure the CSS of RBC output under near-physiological conditions. (**B**) Pairs of highly overlapping A17 amacrine cells contact many of the same RBCs but at different synaptic locations (arrows). Same RBC serial EM reconstruction as in ***Figure 1*** but with an additional reconstructed A17 amacrine cell dendrite from a different A17 (AII is removed). (**C**–**E**) Paired recordings from neighboring A17 amacrine cells revealed strong covariation in excitatory synaptic input from RBCs under dark-adapted conditions. Dim backgrounds increased presynaptic release (**C**) but decreased correlated activity in neighboring A17 amacrine cells (**D** and **E**; $p = 0.0053$ for change relative to dark, $n = 8$ pairs). Upon returning to darkness for ~2 min the strong covariation of presynaptic input recovers to that observed before the background was presented. (**E**) Population data for cross-correlation functions in darkness (left), 0.5 R*/rod/s (middle) and after returning to darkness (i.e. recover, right). Thick lines represent the mean, shaded regions represent ±SEM.

DOI: 10.7554/eLife.03892.004

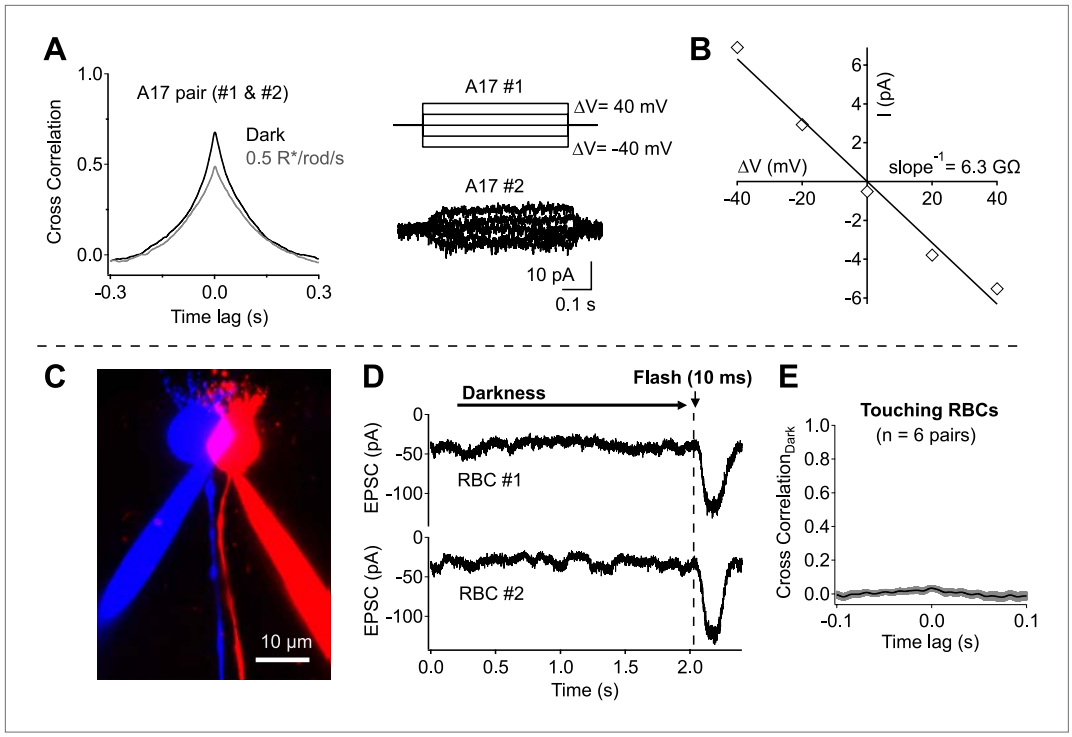

Figure 3. Network divergence and electrical coupling only weakly contribute to correlations observed in highly overlapping A17 amacrine cells. (**A** and **B**) Overlapping A17s exhibit weak electrical coupling. (**A**) Example recording: strong correlations are observed in overlapping A17 amacrine cells (left), even in the absence of significant electrical coupling (right). (**B**) The gap junctional resistance was estimated by determining the slope of the ΔV-I relationship. (**C**–**E**) Dendritic input to neighboring RBCs is only weakly correlated in darkness. (**C**) Confocal reconstruction of a paired recording from RBCs with touching somas. (**D**) Example traces from touching RBC pair. Each recording trial consisted of 2 s of complete darkness followed by a 10 ms flash (to monitor sensitivity). (**E**) Cross correlations were derived for each recording pair before averaging across cells (mean ± SEM). These experiments were conducted using wild-type retinal slices.

DOI: 10.7554/eLife.03892.005

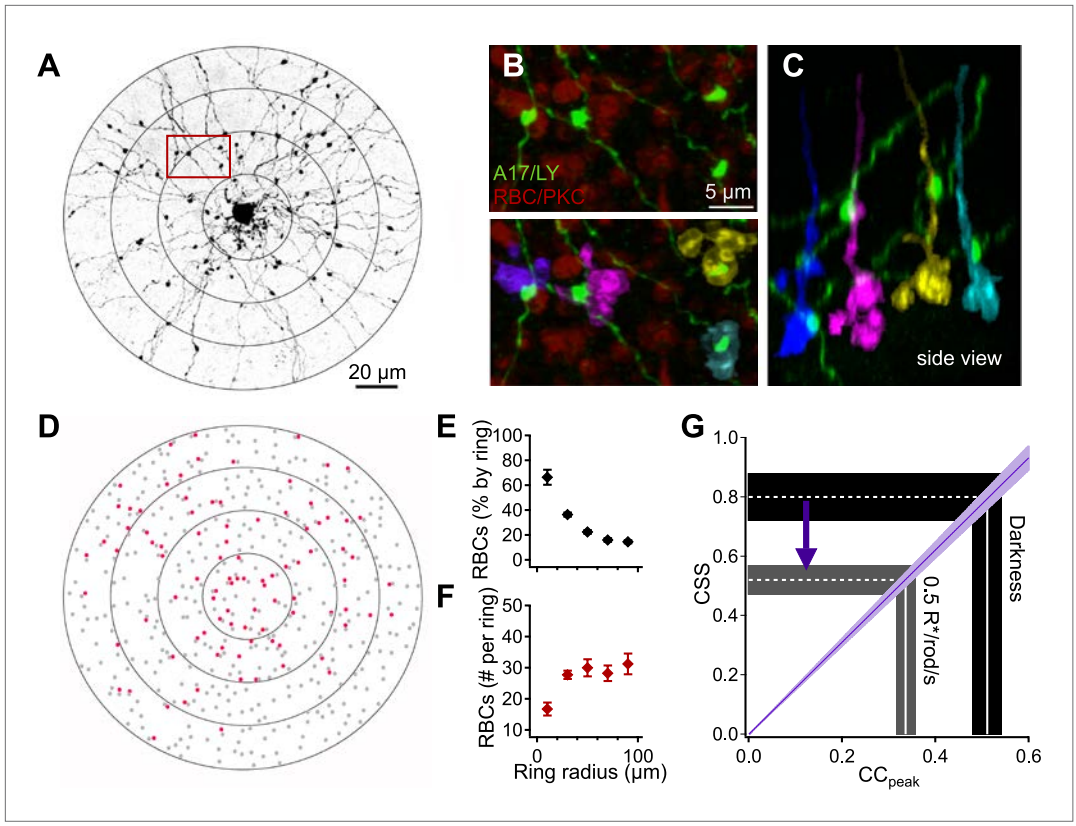

Figure 4. Interpreting A17-A17 correlations in terms of RBC cross-synaptic synchrony. A17 amacrine cell-RBC connectivity was assessed using immunohistochemistry and single-cell injections. (**A**) A17 amacrine cells have long, thin neurites that are studded by synaptic varicosities. Connectivity between RBCs and Lucifer-yellow (LY) injected A17s were determined within 20 µm concentric rings centered on the soma of the injected A17 cell. The outermost ring from panels **A** and **D** was removed from the image for better viewing of the proximal dendrites but were included in all analyses. (**B**) Inset from **A**, RBCs were labeled using antibodies against PKCα (red). Synapses between the RBC and A17 cells were identified by sites of appositions between A17 varicosities and the RBC axon terminal (see 'Materials and methods'). Axonal boutons of four RBCs are colorized separately. (**C**) Orthogonal rotation of the image stack showing a side view of the four RBC axon terminals connected to the A17 amacrine cell in **A** and **B**. (**D**) Connectivity map for the A17 cell example in **A**. Red dots represent the axons of connected RBCs, and gray dots represent the axons of RBCs that did not contact the A17. The percentage (**E**) and number (**F**) of RBC connections was determined as a function of radial distance for four injected A17s from four different animals. A17 dendrites traverse ~40 µm of the inner plexiform before reaching sublaminas 4 and 5 (where they make the majority of their synaptic contacts with RBCs), therefore, the most central concentric ring actually corresponds to dendritic distances between 40 and 60 µm, the second ring corresponds to dendritic distances between 60 and 80 µm and so on. (**G**) Changes in the peak amplitude of the cross correlation function reflect luminance-dependent changes in cross-synaptic synchronization as determined by the connectivity and ***Equation 1*** (purple line). Data are presented as mean ± SEM; SEMs are represented by error bars (**E** and **F**) or shaded regions (**G**). These anatomical experiments were conducted on whole mount retinas taken from *Igfbp2*-GFP mice. Also see ***Figure 4—figure supplement 1***.
DOI: 10.7554/eLife.03892.009

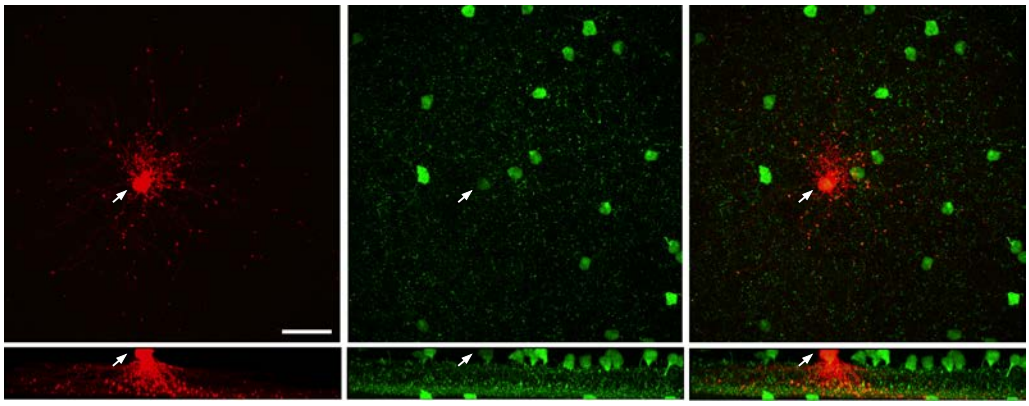

Figure 4—figure supplement 1. Images from *Igfbp2*-GFP C57BL6 retina. (*left*) Image of a single A17 (anti-lucifer yellow, red) injected with lucifer yellow. White arrow points to the soma, scale bar is 30 μm. (*middle*) GFP-positive cell bodies (anti-GFP, green) are present in both the inner nuclear layer and ganglion cell layer in this line. (*left*) Merged image of the GFP positive A17 cell.

DOI: 10.7554/eLife.03892.010

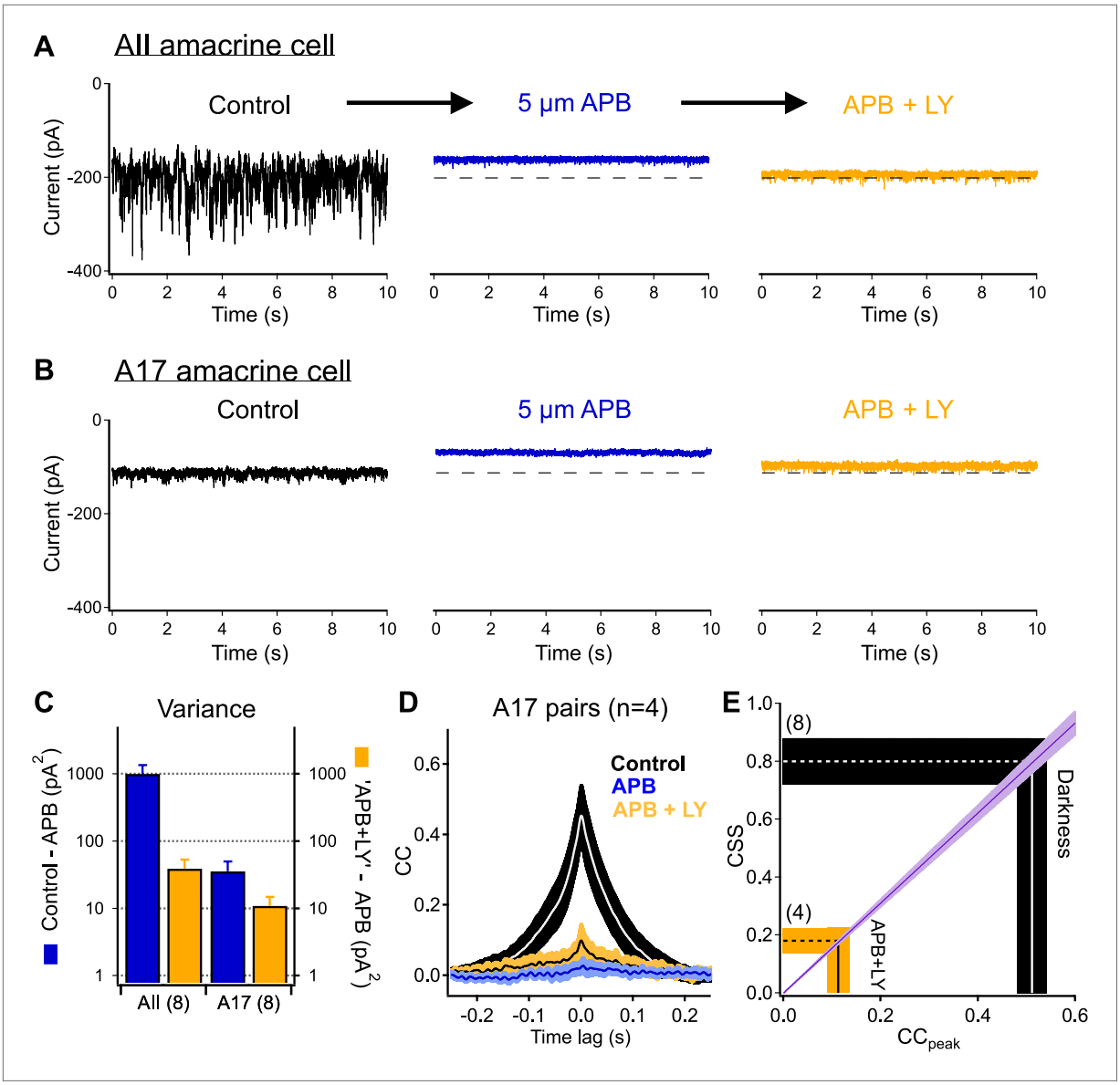

Figure 5. Highly synchronized synaptic noise at RBC→AII connections under dark-adapted conditions is driven by upstream rod-dependent noise. (**A**–**B**) mGluR6 agonists and antagonists can be used to override rod→RBC synaptic connections and probe cross-synaptic release properties at RBC→AII connections. Application of the mGluR6 agonist APB (5 μM, *blue-middle*) hyperpolarizes the RBCs and shuts down synaptic transmission (i.e., output) to the postsynaptic AII (**A**) and A17 (**B**) amacrine cells. Addition of the mGluR6 antagonist LY (0.5–2 μM, *yellow-right*) restores tonic release from RBC output synapses (i.e., similar holding current), however, RBC output synapses are now insensitive to fluctuations in transmitter release between rods and RBCs. (**C**) Summary graph comparing network noise properties observed by AII and A17 amacrine cells (n = 8 for all bars). The AII amacrine cell inherits (from RBCs) an order of magnitude more network noise than the A17 amacrine cell (*blue*: $\sigma^2_{Con} - \sigma^2_{APB}$) but recovers only a small fraction of this noise when tonic release from RBC synapses is restored (*yellow*: $\sigma^2_{LY+APB} - \sigma^2_{APB}$). (**D**) Bath application of 'APB' and 'APB + LY' strongly suppress correlated activity in overlapping A17s (APB: p = 0.0088 for change relative to dark; APB + LY: p = 0.0034 for change relative to dark; n = 4 pairs). (**E**) Although the majority of tonic presynaptic glutamate release can be recovered in the presence of 'APB + LY', CSS measurements indicate that RBC output synapses are highly desynchronized under these conditions, thus partially explaining the differences in recovered variance in the AII and A17 amacrine cells. Also see ***Figure 5—figure supplement 1***.

DOI: 10.7554/eLife.03892.006

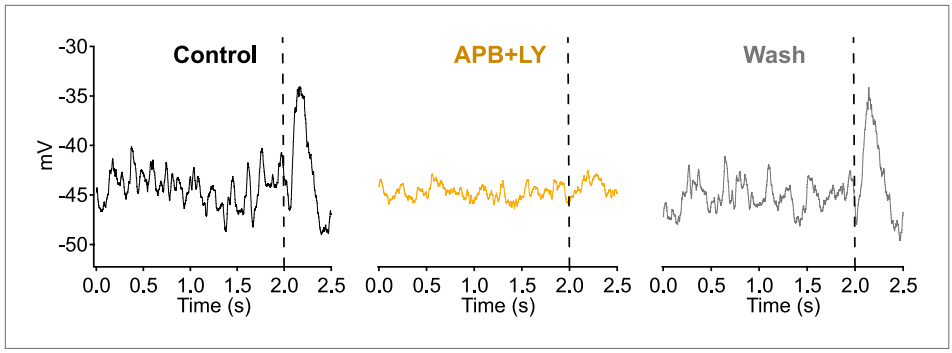

Figure 5—figure supplement 1. Bath application of a solution containing 1 μM LY341495 and 5 μM APB suppresses dendritic input and voltage fluctuations in RBCs. 2 s of dark record were collected in current clamp before delivering a dim 10 ms flash to monitor sensitivity (vertical dashed line).

DOI: 10.7554/eLife.03892.007

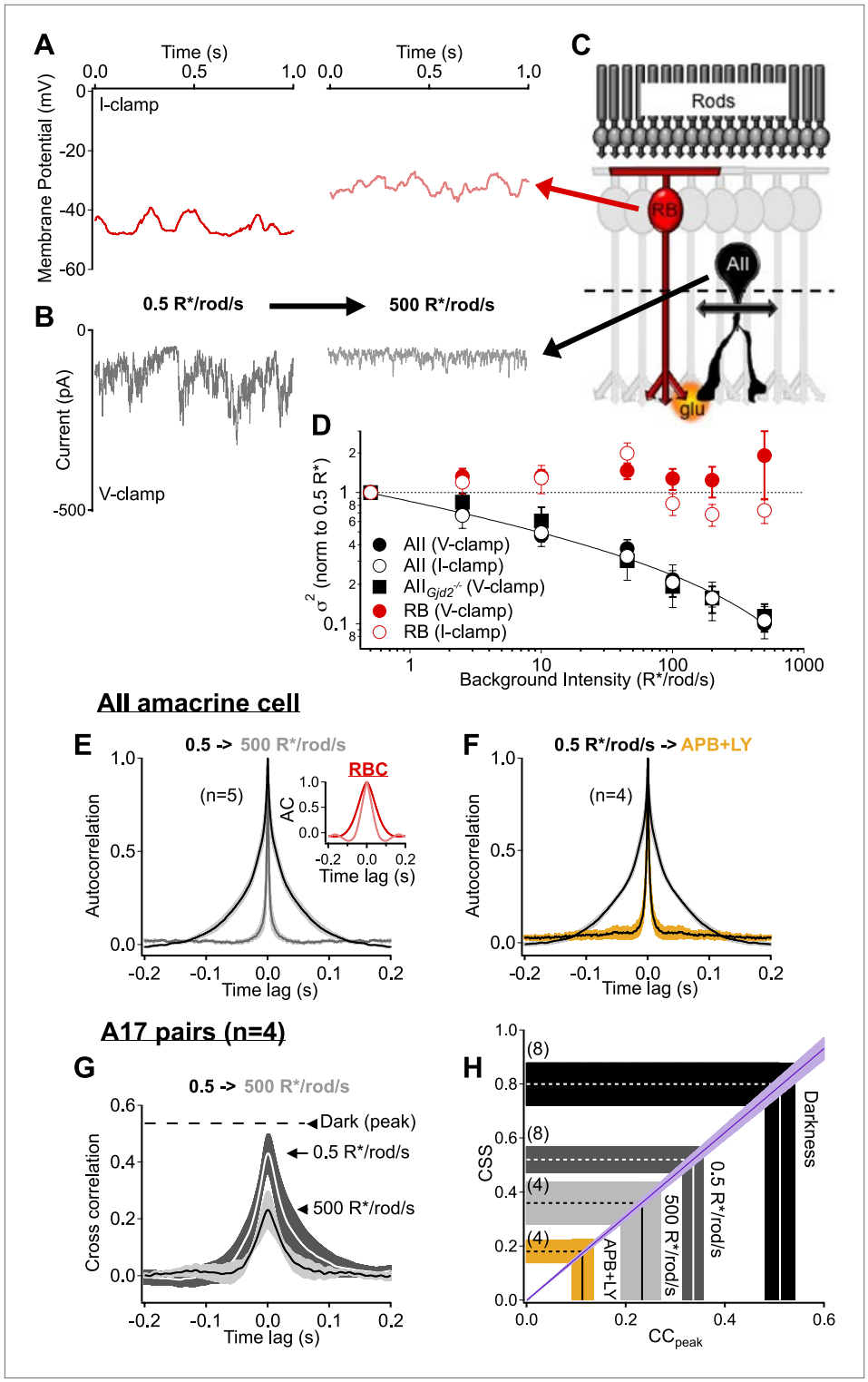

Figure 6. Rod bipolar cell output synapses continue to desynchronize with increasing luminance, reducing the transmission of rod-dependent noise at higher backgrounds. (**A**–**C**) Individual recordings from a RBC (**A** and **C** red) and AII amacrine cell (**B** and **C** *black*) in the presence of a dim background (0.5 R*/rod/s, left) and 1000-fold brighter background (right) illustrate the noise reduction across the RBC. (**D**) Population data for voltage-clamp recordings of excitatory synaptic input and current clamp recordings of membrane signaling in RBCs (*red*) and AII amacrine cells (*black*). Noise recorded from RBCs remained relatively constant across this range of backgrounds (comparison

Figure 6. Continued on next page

Figure 6. Continued

of noise at 500 relative to 0.5 R*/rod/s, V-clamp: p = 0.92, n = 7; I-clamp: p = 0.18, n = 4) while noise recorded from AII amacrines was reduced ~10-fold (comparison of noise at 500 relative to 0.5 R*/rod/s, V-clamp: p = 0.0039, n = 5; I-clamp: p = 0.019, n = 5). AII amacrine cell recordings from the retinas of mice lacking connexin36-containing gap junctions (*black* squares) indicate that neither gap junctions, nor the secondary rod pathway, are required for this transition (comparison of noise at 500 relative to 0.5 R*/rod/s, V-clamp: p = 0.017, n = 5). Error bars represent ± SEM across cells. (**E**) Average autocorrelation functions for a population of AII amacrine cells recordings under steady-state illumination at 0.5 and 500 R*/rod/s. Slower temporal correlations in the input currents are strongly reduced in the AII amacrine cell across this range of luminance. Inset: the reduction in temporal correlations of the RBC voltage response is much less than that observed in the AII. (**F**) The 'LY+APB' manipulation greatly reduces temporal correlations in RBC output, similarly to adaptation to 500 R*/rod/s. (**G**–**H**) Paired-recordings from A17 amacrine cells reveal that RBC output synapses become increasingly desynchronized/independent as the retina is adapted to higher luminance (CC_{peak} = 0.23 ± 0.05 at 500 R*/rod/s vs 0.54 ± 0.06 in darkness, n = 4 pairs, p = 0.029). Taken together these data indicate that RBC synapses desynchronize and reduce rod-dependent noise transmission when the retina is adapted to brighter conditions, when the cone-driven circuits are beginning to convey more of the visual information. Thick lines represent means, shaded regions represent ±SEM.

DOI: 10.7554/eLife.03892.011

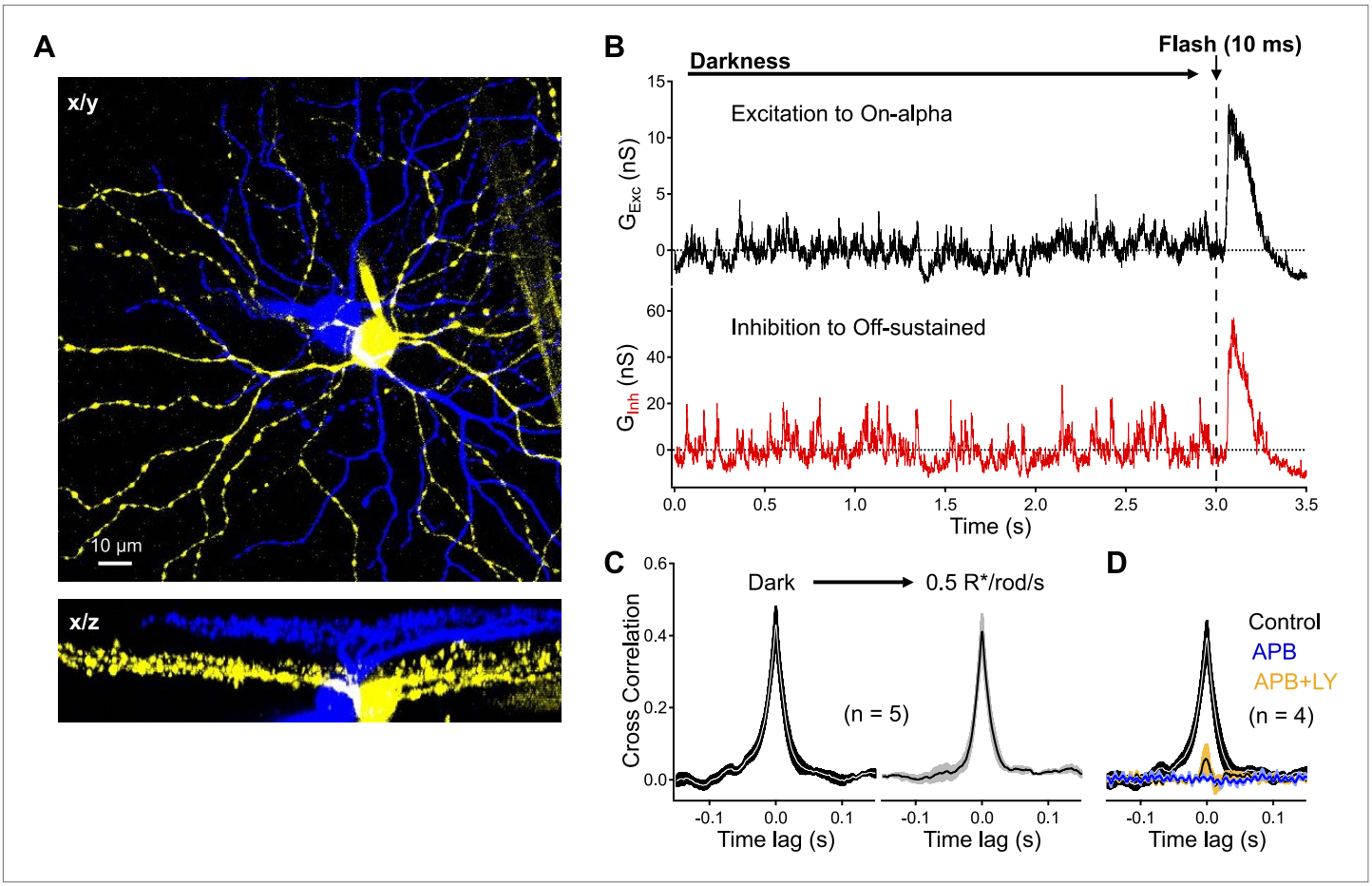

Figure 7. Dark noise and CSS drive strongly-correlated synaptic activity in highly-overlapping On alpha - OFF sustained ganglion cell pairs. (**A**) Confocal reconstruction of a paired recording from an On alpha (*yellow*) and OFF sustained (*blue*) ganglion cell. (**B**) Example traces of simultaneous recordings of excitatory input to an On alpha (*black*) and inhibitory input to an Off sustained (*red*) ganglion cells. At the end of each recording epoch a brief flash was delivered to monitor sensitivity over time. (**C**) Peak cross correlations measurements from five pairs indicate that synaptic activity is slightly more correlated in the darkness than in the presence of a dim constant background ($p = 0.037$ for a change in CC_{peak} relative to dark, n = 5 pairs). (**D**) Suppression of outer retinal activity transmission with APB (5–10 µM) eliminates ganglion cell correlations ($p = 0.0048$ for change in CC_{peak} relative to dark, n = 4 pairs). Additional application of LY (at similar concentrations to ***Figure 5***) produces weak correlations in the pairs ($p = 0.0089$ for a change in CC_{peak} relative to dark, n = 4 pairs). Thick lines represent means, shaded regions represent ±SEMs. These experiments were conducted using wild type whole mount retinal preparations.

DOI: 10.7554/eLife.03892.012

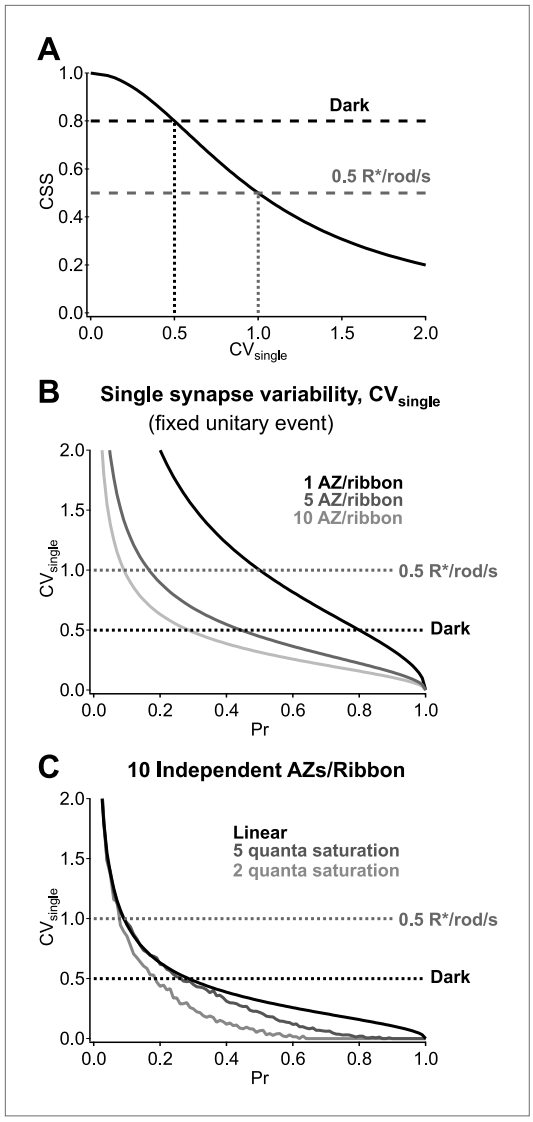

Figure 8. Multiple active zones (AZ) per synapse and low synaptic variability enhance CSS in darkness. (**A**) CSS measurements constrain synaptic variability at individual synaptic connections. Assuming a homogeneous release probability, a CSS measurement of 0.8 in darkness indicates that the coefficient of variation (CV) at individual synapses must be ≤0.5. (**B**) Multiple release sites/active zones improve reliability at individual synapses. Previous work indicates that each RBC ribbon synapse has ~10 active zones, thus facilitating multi-vesicular release. (**C**) Postsynaptic receptor saturation can further improve reliability at individual synapses. If the synaptic receptors are saturated by the release of five or more vesicles (dark gray) then the response to the release of >5 vesicles will be identical to the response to five vesicles. This reflects a tradeoff between dynamic range and reliability.

DOI: 10.7554/eLife.03892.008